Backward emission of energetic protons

M. Avan, A. Baldit, J. Castor, G. Chaigne, A. Devaux, J. Fargeix, P. Force, G. Landaud, G. Roche, and J. Vicente
Laboratoire de Physique Corpusculaire, Université de Clermont-Ferrand II, 63170 Aubiere, France

J. P. Didelez and F. Reide
Institut de Physique Nucléaire, 91406 Orsay, France

S. A. Gurvitz
Department of Physics, Weizmann Institute of Science, 76100 Rehovot, Israel
(Received 28 October 1983)

Inclusive cross sections for energetic protons emitted at backward angles were measured using a 200 MeV proton beam bombarding ^{6}Li, ^{27}Al, ^{58}Ni, and ^{197}Au targets. The data were analyzed using the quasi-two-body scaling approach. It is shown that a scaling regime is reached for some of the data taken at incident energies of about 200 MeV/nucleon. This regime, however, is different from the one observed above 600 MeV/nucleon.

I. INTRODUCTION

In the past decade, a large amount of experimental work has been devoted to investigating the momentum distribution of nucleons or clusters in nuclei. The knockout reactions, considered as quasi-free scattering on a nucleon or a cluster, have been most commonly used. Such quasi-elastic processes preferentially probe low momentum components of the distributions up to 300 MeV/c,[1] but much larger momenta (1 GeV/c) are known to be present in nuclear matter, from theoretical (short range correlation[2]) as well as experimental[3] (large momentum transfers) considerations. However, their direct measurement has remained so far unclear or questionable, and in many cases strongly model dependent.

Recently, the backward emission of energetic particles could be directly related to the high momentum components in nuclear matter through the quasi-two-body scaling (QTBS) model.[4–6] In this framework, a large amount of data taken with projectiles having more than 600 MeV/nucleon could be reproduced[6] with a "universal" momentum distribution, confirming quantitatively the initial ideas of Frankel.[4,7]

In the present work we investigate energetic protons emitted backwards resulting from the interaction between various targets and 200 MeV protons. At this incident energy, the N-N scattering cross section has reached its minimum value and the threshold for π production is barely reached. This should favor mechanisms simpler (i.e., with a small number of interactions) than those occurring at energies around and above the (3,3) resonance, and consequently provide "cleaner" results.

Roughly speaking, if a projectile proton is scattered backward with little energy loss after a single scattering on a nucleon of the target, this target nucleon must have had, before the collision, a large Fermi momentum. Pure kinematical relations fix minimum and maximum values of this momentum ($k_{\min}$ and $k_{\max}$), which depends solely on the angle and outgoing energy of the observed proton.[5,6] In the QTBS picture, the backward scattering cross section can be related to the probability for the target nucleons to have a Fermi momentum larger than $k_{\min}$ and smaller than $k_{\max}$.

In the present experiment, cross sections for the highest outgoing energies (close to the maximum kinematic limit) have been purposely investigated to emphasize the above-mentioned mechanism. Cascade codes indeed show that large outgoing energies always result from a small number of interactions. Even at the moderate backward angle of 100°, we are dealing with large $k_{\min}$ values, far above the quasi-free scattering range. It is thus interesting to compare our experimental results with the QTBS prediction.

In Sec. II, we describe the experimental setup. Section III is devoted to the experimental results. In Sec. IV we compare the data with QTBS predictions and the cascade model, and finally we give the conclusion in Sec. V.

II. EXPERIMENTAL SETUP

The 200 MeV proton beam extracted from the Orsay Synchrocyclotron is focused on a target spot of 2×4 mm^2. Various targets (^{6}Li, ^{27}Al, ^{58}Ni, and ^{197}Au) were used as representatives of light, medium, and heavy nuclei.

Most of the experimental setup is described in detail in

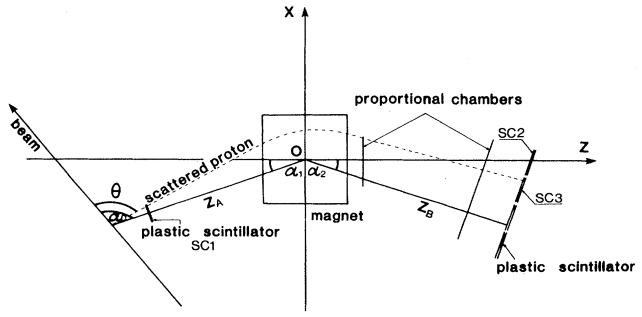

FIG. 1. Schematic arrangement of the detectors and the bending magnet.

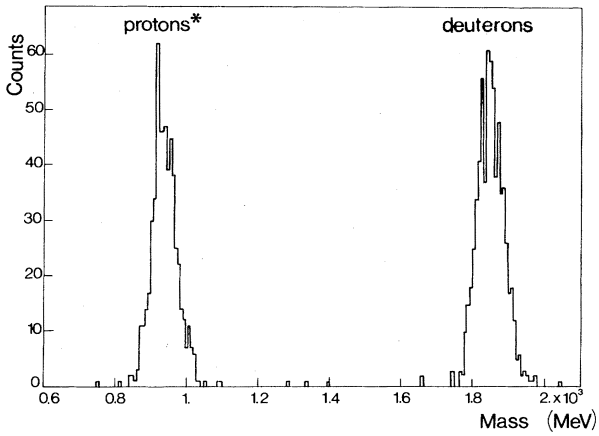

FIG. 2. Particle identification by a time-of-flight technique. (*) scale divided by 1000 for protons (^{197}Au target).

Refs. 8 and 9 and has been used as a proton detector in previous experiments involving (p-γ) coincidences.[10] As shown in Fig. 1, it mainly consists of a large acceptance magnet, large both in momentum (300—700 MeV/c) and angle ($\sim 10°$). Two multiwire proportional counters (MWPC's) behind the magnet provide the necessary information to reconstruct trajectories, while particle identification is accomplished by a time-of-flight technique (Fig. 2). After processing the data, the three pieces of information obtained for each event are the following: particle identification, and scattering angle and momentum of the detected particle. The angular uncertainty is better than 2 mrad. The momentum resolution $\Delta p/p$ is about 5×10^{-3}.

All those characteristics are more than sufficient to investigate inclusive proton spectra and should provide more reliable results than those usually obtained with range telescopes. In order to check all calibrations (momentum, acceptance, and efficiency), runs at forward angles were done with CH_2 targets to measure the p-p cross sections, before moving the whole system towards the backward region.

Inclusive proton spectra were measured at 102° and 106° for outgoing protons with an energy range extending from 80 MeV to the maximum kinematic limit. In some cases, to avoid prohibitive counting rates from the low energy portion of the spectra, absorbers were introduced close to the SC1 plastic scintillator (Fig. 1) to limit the data processing to protons having more than 120 MeV.

The beam intensity was measured with an absolute accuracy better than 3% by a Faraday cup buried in the beam-catcher concrete wall.

III. RESULTS

The inclusive proton spectra taken at a mean angle of 102 deg are displayed in Fig. 3 for ^{6}Li, ^{27}Al, ^{58}Ni, and ^{197}Au, respectively. The inclusive proton spectra are very sensitive to the mean angle for all targets. Figure 4 shows this variation for a ^{27}Al target when the mean angle varies from 102 to 106 deg. Errors bars, purely statistical, are shown when larger than the points.

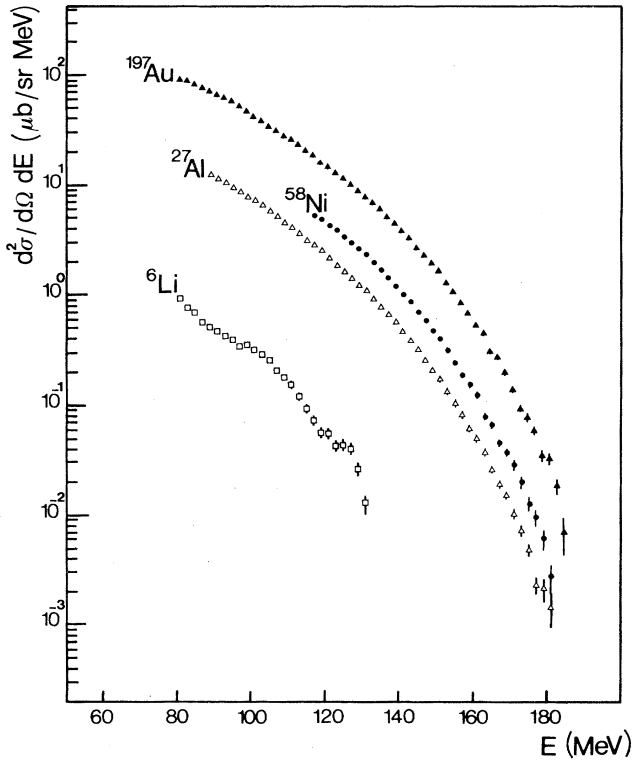

FIG. 3. Inclusive proton spectra as a function of outgoing proton energy at mean angle (102°) for ^{6}Li (□), ^{27}Al (△), ^{58}Ni (●), and ^{197}Au (▲).

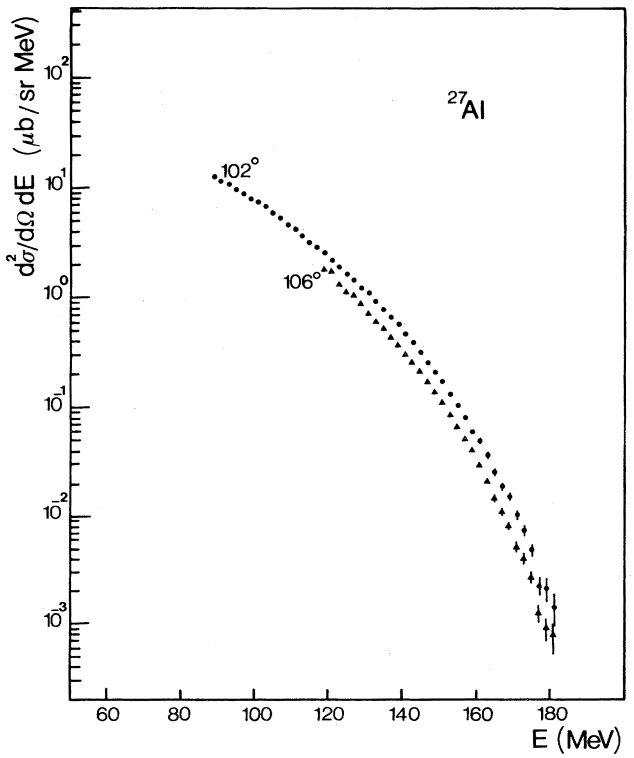

FIG. 4. Inclusive proton spectra as a function of outgoing proton energy for ^{27}Al at mean angles 102 (●) and 106 (▲) deg.

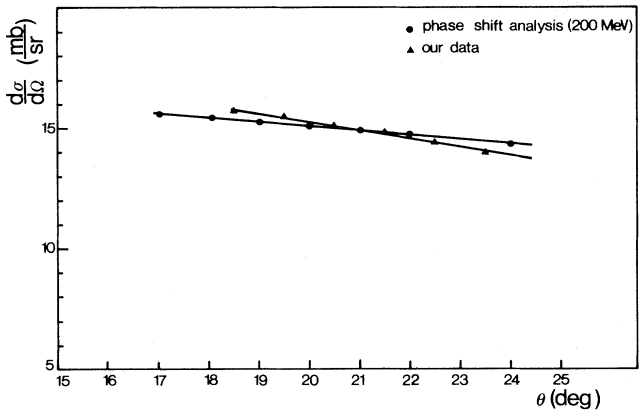

FIG. 5. Proton-proton elastic scattering differential cross sections as a function of the scattering angle. (▲), our data. (●), phase shift analysis (200 MeV).

For all targets, except ^{6}Li, the overlap between data taken in two different runs, six months apart, was within the error bars. The introduction of an absorber to cut the low-energy particles did not distort the high energy behavior of the spectra.

The uncertainty in absolute normalization due to target thickness, beam monitoring, and efficiency of the system as a function of proton energy (by far the largest contribution) is estimated to be lower than $\pm 5\%$. We have tested our experimental setup with a polyethylene target (CH_2) and we have obtained the pp elastic scattering $d\sigma/d\Omega$ (mb/sr) at 200 MeV incident energy for different angles (18°–24°). Our experimental data are in good agreement with those calculated from phase shift analysis[11] (Fig. 5).

Our spectra are also in agreement in absolute value and shape, within quoted errors, with other data taken with completely different experimental setups. At 200 MeV on ^{27}Al and ^{197}Au and at 198 MeV on ^{58}Ni,[13] proton spectra were measured with a stack of germanium detectors.[12] For example, the cross section 8.8 μb/MeV sr, obtained with our experimental results in the following case, incident proton energy 200 MeV; mean angle 102 deg; outgoing energy 128.4 MeV; ^{197}Au target, is in good agreement with the value of 10 μb/MeV sr deduced from a linear extrapolation of the data obtained in Ref. 12.

The general behavior of the data is described by a smooth falloff somewhat faster than an exponential one, except in the ^{6}Li case, where we observe a hump in the cross section between 95 and 115 MeV. This can be explained by the characteristic structure of ^{6}Li. Indeed, the well-known tendency of this particular nucleus to cluster in an $\alpha+$d structure may induce, by backward elastic scattering on one cluster, extra bumps in the spectra. A simulation program for a (p,pα) reaction on ^{6}Li was performed for our experimental conditions. The corresponding proton distribution points around 95—115 MeV.

For all targets, the kinematic limit has been approached with protons currently detected up to 180 MeV.

IV. THEORETICAL INTERPRETATION

The inclusive spectra of energetic protons emitted at backward angles can be analyzed in terms of QTBS. In the most recent theoretical approach developed by Gurvitz,[5,6] a large amount of data $pA\to p'X$, $A_1A_2\to p'X$ obtained for impinging energy 0.6—1.0 GeV/nucleon and $90°\le\theta'_p\le 180°$ are remarkably well reproduced using a universal one nucleon momentum density distribution $n(k)$, which appears to be the same for medium and heavy nuclei ($A\gtrsim 20$). This approach disregards rescattering of the projectile on target nucleons, assuming the dominance of the single scattering mechanism in the large angle inclusive reactions. However, other effects such as the final state interaction (FSI) of nuclear fragments, binding potential effects in the scattering on a bound nucleon, and projectile-nucleon Pauli interchange effects are taken into account.[5,6] As a result, the experimental inclusive cross sections are expressed in terms of *on-shell* pp,pn cross sections and a quantity $G(k_{\min})$.

$$\frac{d^2\sigma_{pA\to p'X}}{dE_{p'}d\Omega_{p'}}=\frac{m(P_L^{\rm eff})^2}{4\pi^2}\frac{p'}{p}\left[Z\frac{d\sigma_{pp}(E_L^{\rm eff},q^2)}{dq^2}+(A-Z)\frac{d\sigma_{pn}(E_L^{\rm eff},q^2)}{dq^2}\right]\frac{G(k_{\min})}{|\vec{p}-\vec{p}\,'|}\,, \tag{1}$$

where

$$G(k_{\min})=\frac{1}{\pi}\int_{k_{\min}}^{\infty}n(k)k\,dk \tag{2}$$

is the integrated one-nucleon momentum distribution. Here $n(k)$ is normalized as

$$\int n(k)d^3k/(2\pi)^3=1\,.$$

The momentum $k_{\min}$ is the minimal momentum of the struck nucleon N in the reaction

$$p+N\to p'+N'\,,$$

where the struck nucleon (and also the projectile) is *on mass shell* before and after collision.[6] It yields

$$\vec{k}_{\min}=-\frac{\vec{q}}{2}\left[1-\frac{\nu}{|\vec{q}|}\left[1+\frac{4m^2}{\vec{q}^{\,2}-\nu^2}\right]^{1/2}\right], \tag{3}$$

where $\vec{q}=\vec{p}-\vec{p}\,'$ and $\nu=E_p-E_{p'}$ are the momentum and energy transfers from projectile to the nucleus, and $\vec{p}$ and $\vec{p}\,'$ are the initial and final momenta of the projectile in the nucleus laboratory frame. The on-shell pp,pn cross sections in Eq. (1) are taken at effective projectile laboratory kinetic energy[5,6]

$$E_L^{\rm eff}=E_L\left[1+\frac{k_{\min}^2}{m^2}\right]^{1/2}-\frac{1}{m}(\vec{p}\cdot\vec{k}_{\min})\,, \tag{4}$$

where $E_L=\sqrt{m^2+p^2}$ is the initial projectile energy. The

effective projectile momentum P_L^{eff} in Eq. (1) is, correspondingly,

$$P_L^{\text{eff}}=\sqrt{(E_L^{\text{eff}})^2-m^2}\ .$$

The large angle proton production spectrum in heavy ion collisions $A_1+A_2\rightarrow p'+X$ is described in the same way, where the projectile nucleus A_1 is considered as a collection of Z_1 protons moving with the same momentum $\vec{p}=\vec{p}_{A_1}/A_1$. Therefore[6],

$$\frac{d^2\sigma_{A_1A_2\rightarrow p'X}}{dE_{p'}d\Omega_{p'}}=Z_1\frac{d^2\sigma_{pA_2\rightarrow p'X}}{dE_{p'}d\Omega_{p'}}\ , \tag{5}$$

where $d\sigma_{pA_2\rightarrow p'X}$ is given by Eq. (1).

Using Eq. (1) the integrated momentum distribution $G(k_{\min})$ can be unambiguously extracted from data points and plotted as a function of $k_{\min}$. The scaling in the $k_{\min}$ variable means that $G(k_{\min})$ extracted from different data sets goes over to the same curve.

The essential difference of the present analysis, in terms of QTBS, from that done earlier[4,5] is the inclusion of the FSI of nuclear fragments.[6] It is interesting that the results for the inclusive cross section, obtained with[6] and without[4,5] the FSI, have the same form as Eq. (1) of the present paper. The only difference is that the argument $k_{\min}$ in the integrated momentum distribution $G(k_{\min})$ is replaced by the different argument $k'_{\min}$ if the FSI is neglected.[5] This $k'_{\min}$ is the scaling variable of Frankel,[4] which is the minimal momentum of the $(A-1)$ recoil nucleus in the reaction

$$p+A\rightarrow p'+N+(A-1)\ .$$

In the nonrelativistic limit and for $A\rightarrow\infty$,

$$k'_{\min}=q-\sqrt{2m(\nu+\epsilon_0)}\ , \tag{6}$$

where ϵ_0 is the binding energy of the struck nucleon. On the other hand, the value of the scaling variable $k_{\min}$, Eq. (3), in the same nonrelativistic limit is

$$k_{\min}=\frac{q}{2}\left[1-\frac{2m\nu}{q^2}\right]\ . \tag{7}$$

In the region of the quasi-elastic peak, $\nu=q^2/2m$, both the scaling variable $k_{\min}$ and $k'_{\min}$ (obtained with and without the FSI) are nearly the same: $k'_{\min}\cong k_{\min}=0$. It means that the FSI is not important in this region. However, these variables are quite different if one goes away from the quasi-elastic peak. In the region of large momentum and small energy transfer to the nucleus, like large angle $p+A\rightarrow p'+X$ reactions, $k_{\min}$ is essentially smaller than $k'_{\min}$. Therefore, the analysis of inclusive data which includes the FSI (Ref. 6) results in the much faster falloff of $G(k)$ than the analysis of the same data which neglects the FSI.[4,5]

In Fig. 6 are plotted the integrated distributions extracted from our data and corresponding to the four different targets used in the present experiment. Points corresponding to ^{27}Al, ^{58}Ni, and ^{197}Au are perfectly aligned, indicating that at 200 MeV incident energy, the scaling takes place. However, points corresponding to the very light ^{6}Li nucleus lie much lower than the others.

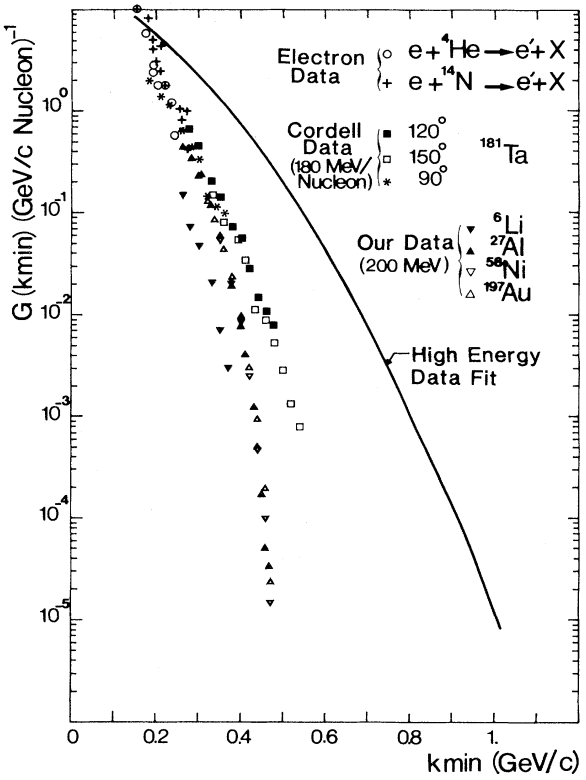

FIG. 6. The solid curve is the "integrated distribution" $G(k_{\min})$ fitting high energy data. The values of $G(k_{\min})$ were obtained from the following: our data (200 MeV proton) for ^{6}Li (▼), ^{27}Al (▲), ^{58}Ni (▽), and ^{197}Au (△) at 102°; the Cordell data (180 MeV/nucleon) for ^{181}Ta at three angles, 120° (■), 150° (□), and 90° (*) (Ref. 14); the electron data for ^{4}He (○) and ^{14}N (+) (Ref. 16).

We have also plotted the integrated distributions extracted from the inclusive proton spectra of Ref. 14 obtained with 720 MeV alpha particles considering the projectile as two protons of 180 MeV, which is comparable to our proton incident energy of 200 MeV. The integrated distributions corresponding to two different targets (^{27}Al and ^{181}Ta) and three scattering angles (90°, 120°, and 150°) fall on the same curve, indicating that in this case also, the scaling takes place. For $k_{\min}$ values smaller than 0.35 GeV/c, the α results agree with the proton ones but lie well below the high energy curve. For $k_{\min}$ values larger than 0.35 GeV/c they disagree more and more, possibly indicating the onset of kinematic limits for our data while coherent transfers may always take place for a projectile as light as an α particle. It should be noted also that the "integrated distribution" extracted from the inclusive proton spectra of Ref. 15 obtained with 90 MeV protons corresponding to three different targets (^{27}Al, ^{58}Ni, and ^{209}Bi) and three scattering angles (90°, 105°, and 120°) shows a scaling comparable to ours.

The large disagreement between the "integrated distribution" obtained at incident energies of the order of 200 MeV/nucleon and those obtained above 0.6–1 GeV/nucleon is somewhat puzzling, since the energy

dependence is taken care of by the theory through the nucleon-nucleon cross section.

The basic assumption of the QTBS concept is that cross sections at backward angle are dominated by a single nucleon-nucleon collision, the projectile proton being scattered at large angle with small energy loss while the other low energy nucleon scattered forward final state interacts with the residual nucleus. This mechanism is possible only if the struck nucleon had a large Fermi momentum and was on shell before the collision,[5,6] and the QTBS analysis of backward cross sections thus provides a measure of the amount of high momentum components.

This approach neglects the multiple scattering of the fast particle. The question is to know in which energy region this is legitimate. The data obtained with electrons should provide a straightforward answer since electrons undergo only the single scattering. Unfortunately, there are almost no published data for $e+A \rightarrow e'+X$ in the kinematical region $k_{\min} > 200$ MeV/c for targets $A > 4$, except for $e+{}^{14}N \rightarrow e'+X$ data in Ref. 16. Those measurements correspond to the kinematical region 200 MeV/$c < k_{\min} < 300$ MeV/c and can be directly analyzed with Eq. (1), where pN cross sections are replaced by eN cross sections. The results for the integrated distribution $G(k_{\min})$ found from these data are shown in Fig. 6. [We also plotted $G(k_{\min})$ for ^{4}He extracted from the electron data of the same authors.[16]]

We see that $G(k_{\min})$ from electron data is very similar to the "integrated distribution" obtained from 200 MeV proton data, but it does not correspond to the "integrated distribution" from 0.6—1 GeV proton data. This probably illustrates the major role of the multiple scattering in the production of backward energetic protons at 0.6—1 GeV incident proton energy. When significant multiple scattering cannot take place, either because the target is too light or because only small energy losses are allowed (outgoing energies approaching the kinematic limit), backward cross sections are considerably hindered. One must admit that QTBS analysis generated too many high momentum components to mimic the multiple scattering process. Consequently, one expects that fewer high momentum components would result from the QTBS analysis of high energy data if the multiple scattering process could be correctly taken into account by the theory.

It remains for us to understand why the QTBS approach can reproduce data above 600 MeV/nucleon so well, particularly the mass energy and angle dependence. Part of the answer may lie in the major role played by the initial collision which triggers the scattering and dominates the mechanism. Such a dominance has been recently demonstrated to occur even at medium incident proton energies (100—200 MeV).

Using a different approach we have tried to reproduce the data by means of a conventional cascade model. The

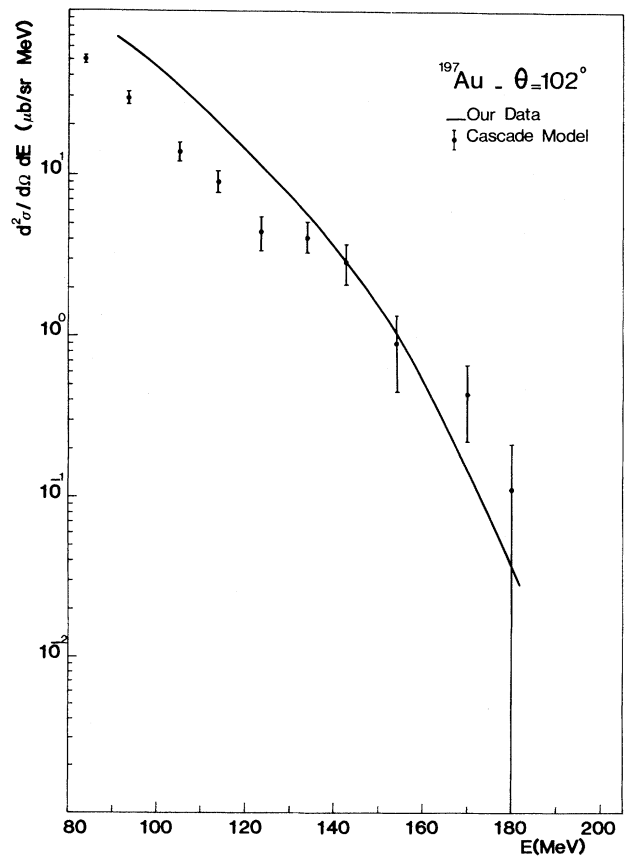

FIG. 7. Solid curve—experimental data. Dots with statistical error: predictions of a cascade for ^{197}Au at mean angle 102°.

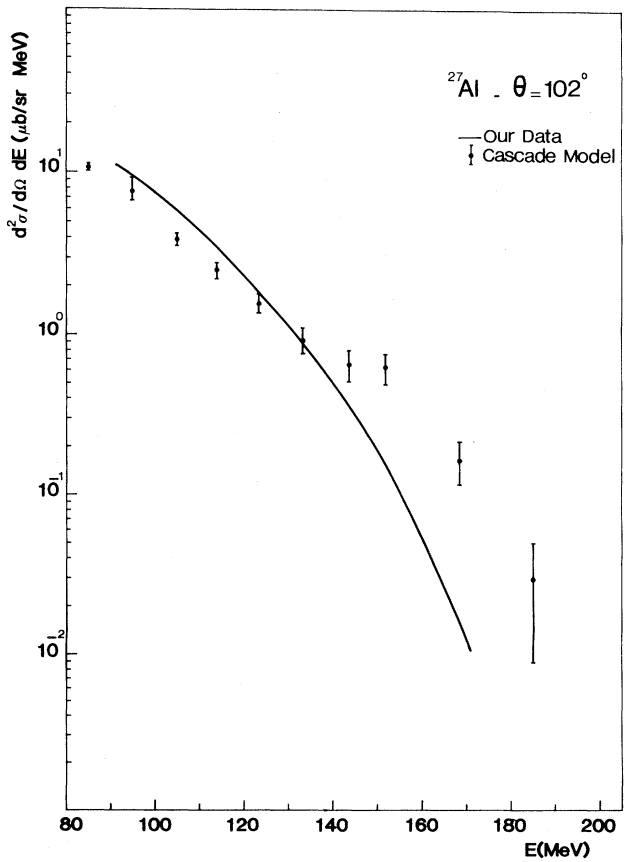

FIG. 8. Solid curve—experimental data. Dots with statistical error: predictions of a cascade code for ^{27}Al at mean angle 102°.

corresponding code is a revised version of the code VEGAS described in Refs. 17 and 18. Several tests have shown that this code gives the same predictions as those obtained by Bertini[18] and Barashenkov *et al.*[19] As a high number of random extractions ($\sim 5\times 10^6$) is necessary to calculate the backward proton cross section, it was necessary to realize a program with a short execution time which is advantageous given the rare events we are dealing with here.

Using only a standard Fermi momentum distribution, it has been possible, as shown in Figs. 7 and 8, to qualitatively reproduce the data. It is of particular interest that in the region of high outgoing energies, the cross sections are significant. They correspond in the Monte Carlo program to a small number of interactions ($\sim 2,3$).

It should also be noted that by studying protons of higher and higher energies for increasing backward angles, interactions with clusters are favored compared to N-N ones, because a small energy loss is required. This mechanism is not taken into account in the theoretical approaches described above.

V. CONCLUSION

Cross sections for backward emission of energetic protons have been measured at 102° and 106° using ^{6}Li, ^{27}Al, ^{58}Ni, and ^{197}Au targets. An interpretation of the data in terms of the most updated QTBS theory taking into account the FSI had been attempted. The scaling observed at incident energies higher than 600 MeV/nucleon is also present at 200 MeV. Such is also the case for data of Refs. 14 and 15 taken at 180 and 90 MeV/nucleon, respectively.

However, the corresponding "integrated distribution" $G(k_{\min})$ falls off much faster with increasing $k_{\min}$ than the high energy curve. It is argued that in the incident proton range from 100 to 300 MeV, which we are dealing with here, multiple scattering effects should be much smaller than at higher energies. In fact, electron scattering data taken on ^{14}N shows the same scaling as the one we observe. The actual existence of a large number of high momentum components in nuclear matter necessitated by QTBS theory to reproduce high energy data may be questioned. This last hypothesis is reinforced by the fact that conventional cascade models predict large cross sections for backward high energy protons with standard Fermi momentum distributions for the target nucleons.

ACKNOWLEDGMENTS

Two of us, J. Castor and J. P. Didelez, are very grateful to the Department of Physics of the Weizmann Institute of Science for financial support during their stay at Rehovot. The Orsay Synchrocyclotron crew is acknowledged for their dedication to running the machine during all experiments.

[1]Th. A. J. Maris, in *Lecture Presented at the Brentwood Summer Institute on Nuclear and Particle Physics at Intermediate Energies,* Victoria, Canada, 1975, edited by J. B. Warren (Plenum, New York, 1976), p. 425.

[2]J. G. Zabolitzky and W. Ey, Phys. Lett. **76B**, 527 (1978).

[3]Compte-rendus sur le Colloque: Mesure et Inteprétation des Impulsions Elevées dans les Noyaux, Saclay report, 1974.

[4]S. Frankel *et al.,* Phys. Rev. C **18**, 1375 (1978); **18**, 1379 (1978).

[5]S. A. Gurvitz, Phys. Rev. Lett. **47**, 560 (1981).

[6]S. A. Gurvitz, Weizmann Institute of Science Report WIS-82/7 March-Ph, 1982.

[7]S. Frankel, Phys. Rev. Lett. **38**, 1338 (1977).

[8]J. Yonnet *et al.,* Phys. Rev. Lett. **40**, 164 (1978).

[9]C. Lebrun *et al.,* Nucl. Instrum. Methods **165**, 409 (1979).

[10]G. Landaud, A. Baldit, J. Castor, A. Devaux, G. Roche, C. Lebrun, M. Louvel, and J. Yonnet, Nucl. Phys. **A384**, 323 (1982).

[11]J. Bystricky and F. Lehar, private communication.

[12]J. P. Didelez *et al.,* in *Proceedings of the 3rd International Conference on Nuclear Reaction Mechanisms, Varenna, 1982,* edited by E. Gadioli (University of Milano, Milano, 1982), p. 237.

[13]H. Holmgren, private communication.

[14]K. R. Cordell, S. T. Thornton, L. C. Dennis, R. R. Doering, R. L. Parks, and T. C. Schweizer, Nucl. Phys. **A362**, 431 (1981).

[15]J. R. Wu, C. C. Chang, and H. D. Holmgren, Phys. Rev. C **19**, 659 (1979); **19**, 370 (1979).

[16]S. V. Dementiy, Yad. Fiz. **37**, 621 (1983) [Sov. J. Nucl. Phys. **37**, 370 (1983)].

[17]K. Chen, Z. Fraenkel, G. Friedlander, J. R. Grover, J. M. Miller, and Y. Shimamoto, Phys. Rev. **166**, 949 (1968).

[18]H. W. Bertini, Phys. Rev. **131**, 1801 (1963).

[19]V. S. Barashenkov *et al.,* Nucl. Phys. **A187**, 531 (1972).